

Article

Ultrasonic Synthesis of Nanochitosan and Its Size Effects on Turbidity Removal and Dealkalization in Wastewater Treatment

Fitri Khoerunnisa ^{1,*}, Yustika Desti Yolanda ¹, Mita Nurhayati ¹, Firdha Zahra ¹, Muhamad Nasir ², Pakorn Opaprakasit ³, Min-Yee Choo ⁴ and Eng-Poh Ng ^{4,*}

¹ Department of Chemistry, Indonesia University of Education, Setiabudi 229, Bandung 40154, Indonesia; yustika@upi.edu (Y.D.Y.); mita@upi.edu (M.N.); fzahra29@student.upi.edu (F.Z.)

² Research Unit for Clean Technology, Indonesian Institute of Sciences, Bandung 40135, Indonesia; mnasir71@yahoo.com

³ School of Bio-Chemical Engineering and Technology, Sirindhorn International Institute of Technology (SIIT), Thammasat University, Khlong Luang 12121, Pathum Thani, Thailand; pakorn@siit.tu.ac.th

⁴ School of Chemical Sciences, Universiti Sains Malaysia (USM), Minden 11800, Penang, Malaysia; alexandriachoo@gmail.com

* Correspondence: fitri@upi.edu (F.K.); epng@usm.my (E.-P.N.)

Abstract: A detailed study on the synthesis of chitosan nanoparticles under ultrasonication is reported in this paper. By using this simple technique, chitosan particles in nanometer range can be easily prepared without using any harmful and expensive chemicals. The results show that increasing the ultrasonic irradiation time and ultrasonic wave amplitude are the key factors for producing discrete chitosan nanoparticles with narrow particle size distribution. The resulting nanoparticles show superior turbidity removal efficiency (75.4%) and dealkalization (58.3%) in wastewater treatment than the bulk chitosan solid (35.4% and 11.1%, respectively), thus offering an eco-friendly and promising approach for treating wastewater via the coagulation/flocculation process.

Keywords: nanochitosan; ultrasonication; coagulation; turbidity removal; dealkalization



Citation: Khoerunnisa, F.; Yolanda, Y.D.; Nurhayati, M.; Zahra, F.; Nasir, M.; Opaprakasit, P.; Choo, M.-Y.; Ng, E.-P. Ultrasonic Synthesis of Nanochitosan and Its Size Effects on Turbidity Removal and Dealkalization in Wastewater Treatment. *Inventions* **2021**, *6*, 98. <https://doi.org/10.3390/inventions6040098>

Academic Editor: Johannes Schwank

Received: 6 September 2021

Accepted: 6 November 2021

Published: 20 December 2021

Publisher's Note: MDPI stays neutral with regard to jurisdictional claims in published maps and institutional affiliations.



Copyright: © 2021 by the authors. Licensee MDPI, Basel, Switzerland. This article is an open access article distributed under the terms and conditions of the Creative Commons Attribution (CC BY) license (<https://creativecommons.org/licenses/by/4.0/>).

1. Introduction

Wastewater is a global issue that should be carefully handled so as to provide sustainable clean water [1]. The uncontrolled water pollution, that depends on the composition and concentration of pollutants, thus affects the physical (color, temperature and turbidity) and biochemical (chemical and biological demand for oxygen, pH and hardness) properties of water [2]. Therefore, the removal of water pollutants via water treatment is crucial to provide clean water for various needs.

Various methods for treating wastewater such as adsorption, ion exchange, sedimentation and filtration are reported [3,4]. In particular, suspended solid separation involving coagulation and flocculation is one of the well-known approaches in wastewater treatment due to its simplicity, high efficiency and low-cost operation [5,6]. In this process, the alum and powdered activated carbon are frequently used as the coagulant-flocculant with a total suspended solid (TSS) removal of 85% and 98%, respectively [7,8]. Nevertheless, these materials suffer from several limitations, such as the generation of large quantities of sludge, changing the pH of water, high-cost backwashing operation, and its residual end-product, which is harmful to the aquatic life [1,9,10].

Biopolymers (e.g., chitosan, alginate and cellulose) are natural polymeric materials derived from animal and plant origins. Among them, chitosan is known as a very promising non-toxic, biocompatible and biodegradable material for various water treatment applications [11,12]. Chitosan has a high distribution of amine (-NH₂) and hydroxyl (-OH) groups which are attached to the β-(1-4)-linked D-glucosamine and N-acetyl-D-glucosamine polysaccharide monomers [13]. As a result, these superior arrangements give chitosan high

chemical reactivity and selective adsorption towards some pollutants [14,15]. In addition, chitosan can also be used as an alternative coagulation and flocculation for the removal of many suspensions in wastewater thanks to its high structural stability and high surface reactivity [1,10,16].

Recently, the synthesis of nanometer-scale chitosan has received enormous attention in numerous industries [17]. This is because down-sizing the particle size to nanometer range will exert substantial and new modification to the properties of these materials (e.g., large surface area, high reactivity, improved mechanical properties, etc.) which are important for advanced applications [18,19]. Compared to their micron-sized counterpart, the chitosan nanoparticles are more preferable in the coagulation and flocculation processes due to their high surface contact area that allows efficient and high adsorption capacity for pollutant in suspension [20].

The synthesis of chitosan nanoparticles can be achieved by using several techniques, such as ionotropic gelation [21], microemulsion [22], sol-gel [23] and thermal decomposition [24]. On the other hand, ultrasonication is also another promising technique for preparing finer particles [25]. Unlike other electromagnetic waves, ultrasonic is a very high frequency mechanical wave (>20 kHz) that is able to break the chemical bonds and microaggregates via vibrational shock waves as a source of energy [26]. The use of the ultrasonication method for producing chitosan nanoparticles with an average size of 283 nm has been recently reported [27]. By using this approach, no harmful chemicals are used, thus avoiding tedious washing and purification steps. Nevertheless, the mean particle size of the chitosan nanoparticles is still large and the particle size distribution is relatively broad. Thus, any effort to further improve the existing process for obtaining smaller chitosan nanoparticles for advanced applications is highly appreciated.

This study reports the facile synthesis of chitosan nanoparticles via ultrasonication pathway, where the effects of ultrasonic wave amplitude and irradiation time onto the particle size and distribution were investigated using microscopy and spectroscopy techniques. Furthermore, their coagulant behavior was then tested in water turbidity removal and dealkalization (removal of carbonate, bicarbonate and hydroxide of alkaline earth metals) for wastewater treatment.

2. Materials and Methods

2.1. Materials

Low molecular weight chitosan ($M_v \sim 33,400$ Da) with a nominal degree of deacetylation (85%) was obtained from Bio Chitosan Pty Ltd. (Cirebon, Indonesia). Sodium acetate trihydrate (99%) and acetic acid (99%) were purchased from Sigma-Aldrich GmbH (Saint Louis, MO, USA) while sodium hydroxide (98%) and hydrochloric acid (37%) were procured from Merck GmbH (Darmstadt, Germany).

2.2. Methods

2.2.1. Preparation of Chitosan Nanoparticles

Chitosan nanoparticles were prepared as follows: Typically, a transparent chitosan solution (1.5%) was prepared by dissolving chitosan (1.500 g) in an acetate buffer solution (pH 6.0) where the acetate buffer solution (100.00 g) was prepared using sodium acetate (0.1 M) and acetic acid (0.1 M) solutions. The chitosan solution was then magnetically stirred for 2 h (500 rpm) to allow slow precipitation of chitosan solid. Next, the solid was collected via centrifugation (10,000 rpm, 10 min) before it was further dispersed in an acetate buffer solution (pH 8.01, 3% *w/v* chitosan). The suspension was ultrasonicated using a Q500 sonicator (750 W, 20 kHz, probe diameter = 7 mm) at various times (5, 20, 60 and 120 min) and amplitudes (40–70%), where the pulse intensity microtip was programmed to 1 s on and 1 s off. The resulting solids were isolated from the solution via centrifugation (10,000 rpm, 10 min) and freeze-dried using liquid nitrogen. The nanochitosan samples synthesized using various sonication durations and amplitudes were given codes, as

presented in Table 1. All experiments were performed in triplicate ($n = 3$), and the particle size distribution data are presented as mean \pm standard deviation (S.D.).

Table 1. Sample codes based on duration and amplitude variations.

Sample Code	Duration (min)	Amplitude (%)
NCS1	5	40
NCS2	20	40
NCS3	60	40
NCS4	120	40
NCS5	120	50
NCS6	120	60
NCS7	120	70

2.2.2. Characterization of Chitosan Nanoparticles

The average particle size and distribution of chitosan nanoparticles were measured by using a Zetasizer Nano ZS analyzer (Malvern Panalytical, Almelo, The Netherlands) where the chitosan nanoparticles were dispersed in the acetate buffer solution (pH 8.01, 0.1% w/v chitosan). The amorphous and crystalline characters of pristine chitosan and chitosan nanoparticles were examined using a D8 Advance X-ray diffractometer (Bruker, Oxford, UK) ($2\theta = 5^\circ\text{--}60^\circ$, $\text{CuK}\alpha$ radiation, $\lambda = 0.15406$ nm, 50 kV, 300 mA). The morphological properties of the chitosan nanoparticles were investigated with a JSM-IT300 InTouchScope™ scanning electron microscope (JEOL Ltd., Akishima, Japan) with an accelerating voltage of 30 kV. Prior to analysis, the samples were sputtered and coated with a thin gold layer. The TEM images of chitosan nanoparticles were captured using a Philips CM12 transmission electron microscope operated at 200 kV. The chemical structure and functional groups of the pristine chitosan and chitosan nanoparticles were determined by using a Nicolet iS5 infrared spectrometer (Thermo Scientific™, Waltham, MA, USA) in the wavenumber range of 500–3800 cm^{-1} .

2.2.3. Preparation of Wastewater Samples

The water samples were collected with a plastic container (3 L) from 3 points downstream Citarum river, Indonesia by using the random sampling method. The sample collection at each point was taken thrice in the daytime. All samples were then mixed and stored at 4 °C prior to water treatment study.

2.2.4. Residual Turbidity Removal and Dealkalization Efficiency Studies

The turbidity removal and dealkalization (removal of alkaline earth metal cations) from wastewater were studied at room temperature (27 ± 1 °C) using a JLT 6 flocculator jar tester (VELP model) equipped with 6 paddle stirrers (Usmate Velate, Italy). Initially, chitosan nanoparticles as the biocoagulant (400 mg L^{-1}) were introduced into the wastewater sample (250 mL). The rapid mixing process was maintained at 200 rpm for 1 min, followed by slow mixing at 50 rpm for 20 min. The samples were then allowed to settle down for 40 min, where the formation of floc was observed after coagulation. Next, the residual turbidity was measured using an EZDO TUB-430 turbidity meter (Shanghai, China). For comparison, the same amount of pristine chitosan powder was also used as the control during the treatment process under similar conditions. The turbidity value of the raw wastewater sample was also measured so as to calculate the percentage of residual turbidity removal (Equation (1)):

$$\text{Turbidity removal (in \%)} = \frac{\text{Turbidity}_{\text{raw wastewater}} - \text{Turbidity}_{\text{after treatment}}}{\text{Turbidity}_{\text{raw wastewater}}} \times 100\% \quad (1)$$

The dealkalization of wastewater samples was measured via measuring the alkalinity of the solution after titration using the standard method 2320 [28]. Typically, the treated and

non-treated wastewater samples (10 mL) were titrated with HCl solution (0.1 M) until the final end-point pH was reached; phenolphthalein was used as an indicator. The alkalinity value (expressed in mg/mL as CaCO₃) was calculated using the Equation (2):

$$\text{Alkalinity (mg/mL as CaCO}_3) = \frac{V_{\text{HCl}} \times N_{\text{HCl}} \times 50,000}{V_{\text{wastewater}}} \quad (2)$$

where V_{HCl} and N_{HCl} are the volume (in mL) and normality (N) of HCl, respectively, 50,000 is a conversion factor for changing the normality into the unit of CaCO₃ and $V_{\text{wastewater}}$ is the volume (in mL) of wastewater sample used [28].

3. Results and Discussion

3.1. Particle Size Analysis of Chitosan Nanoparticles

Figure 1a–d shows the particle size distribution of chitosan nanoparticles after irradiation with an ultrasonic wave (ultrasonic amplitude = 40%) for 5, 20, 60 and 120 min. The data show that the ultrasonic treatment initially does not show significant impact on the particle size of chitosan. Within 5 min of ultrasonication, the mean particle size was 426.75 ± 136.12 nm with very broad standard deviation (Figure 1a). Nevertheless, the size reducing effect became more pronounced when the irradiation time was prolonged to 20, 60 and 120 min (Figure 1b–d). The mean size of chitosan nanoparticles (NCS2) was 336.44 ± 82.08 nm after 20 min of treatment before the size further decreased to 220.08 ± 20.60 nm (NCS-3, 60 min) and 109.59 ± 10.11 nm (NCS-4, 120 min). In addition, the effect of ultrasonication on the particle size distribution of NCS was also observed where the NCS-1 (5 min of ultrasonic treatment) initially has a broad size distribution of particles. By prolonging the ultrasonication duration, the particle size distribution of chitosan nanoparticles became narrower, causing a change from bimodal to monomodal particle size distribution. Among the four samples prepared, NCS-4 showed the most uniform and smallest particle size (ca. 110 nm) (Figure 1a). Thus, the data indicate that long exposure of chitosan particles to a very high frequency ultrasonic radiation (>20 kHz) is not only able to break the microaggregates but also can break down the 1,4-glycosidic bonds of chitosan, which may be attained through the high shear forces generated during the ultrasonic treatment [27]. In addition, the heat that is generated during ultrasonication can also contribute to the depolymerization of chitosan through main-chain scissions [29].

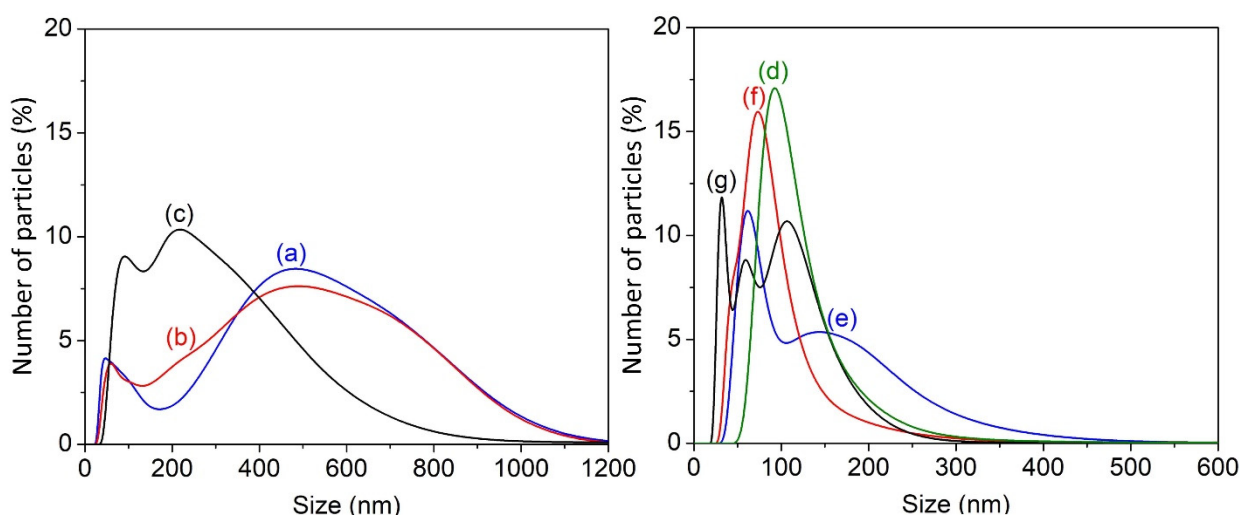


Figure 1. Particle size distribution plots of (a) NCS1, (b) NCS2, (c) NCS3, (d) NCS4, (e) NCS5, (f) NCS6 and (g) NCS7 chitosan nanoparticles.

The ultrasonic radiation amplitude can be another crucial variable affecting the particle size of chitosan nanoparticles. Hence, the synthesis was conducted using different ultrasonic amplitudes (40, 50, 60 and 70%), where the time duration was maintained at 120 min

(Figure 1d–g). The data reveal that the ultrasonic amplitude has less impact towards the particle size distribution of chitosan nanoparticles as compared with the time duration. This is because an increased amplitude may produce more cavitations, which reduce the efficiency of energy transmission and further reduce the effect of ultrasonication [30,31]. Narrow particle size distribution can be seen in the NCS4, NCS5, NCS6 and NCS7 samples, ranging from 50 nm to 150 nm. On the other hand, the mean particle size also showed slight decrease from ca. 110 nm to 77 nm upon increasing the ultrasonic amplitude from 40% to 70% (Table 2). Thus, the data indicate that the intermolecular chemical bonds of chitosan biopolymer could be cleaved by increasing the amplitude of vibrational shock waves as an external source of energy [26]. Regarding pristine chitosan, DLS was unable to detect its particle size distribution due to its macro-particle size (data not shown).

Table 2. Mean diameter and standard deviation of chitosan nanoparticles synthesized using different ultrasonication amplitudes and durations.

Sample Code	Duration (min)	Amplitude (%)	Mean Diameter (nm)
NCS1	5	40	426.75 ± 136.12
NCS2	20	40	336.44 ± 82.08
NCS3	60	40	220.08 ± 20.60
NCS4	120	40	109.59 ± 10.11
NCS5	120	50	110.32 ± 36.27
NCS6	120	60	79.33 ± 21.61
NCS7	120	70	77.47 ± 28.81

Mean ± S.D., $n = 3$.

3.2. FTIR Spectroscopy Analysis

FTIR spectroscopy is a sensitive technique and hence it was used to identify the change in the functional groups and molecular structure of chitosan samples [32]. Figure 2 shows the IR spectra of pristine and nanosized chitosan samples. For pristine chitosan, a very broad band due to the O–H group was observed at 3300–3600 cm^{-1} . Upon increasing the ultrasonication time, this region became more resolved and split into three bands; the band at 3406 cm^{-1} is due to O–H stretching mode while the bands at 3273 and 3178 cm^{-1} are attributed to the primary N–H groups [33]. This phenomenon can be explained by the breakdown of intramolecular hydrogen bonds at chitosan nanoparticles compared to that of bulk chitosan by which the bulk chitosan has more intramolecular hydrogen bonds in long-chain chitosan polymers [34]. In addition, a decrease of intensity of a band at ca. 1066 cm^{-1} (due to C–O–C group) was also detected, especially for the samples treated for more than 60 min with >40% amplitude (NCS2–NCS7). This observation indicates the rupture of the β -glycosidic-linkages between the glycosamine and N-acetylglucosamine moieties after long exposure of ultrasonic wave with high amplitude [35]. As a result, smaller chitosan particles are formed. Meanwhile, no significant change and shifting are observed after the synthesis for the IR bands at 2872 cm^{-1} (C–H stretching), 1642 cm^{-1} (N–H bending), 1550 cm^{-1} (CO_2Na), 1414 cm^{-1} (C–H asymmetrical bending), 1347 cm^{-1} (C–H symmetrical bending), 1143 cm^{-1} (C–O) and 1021 cm^{-1} (C–O) [36]. In addition, the FTIR spectroscopy results do not show any new absorption peaks for the chitosan nanoparticles, indicating that ultrasonication is a physical method that does not change the composition and structure of chitosan [37].

3.3. Morphological and Crystallinity Analyses

The X-ray diffraction (XRD) technique can reveal the effect of ultrasonication on the crystallinity and structural properties of chitosan particles. In respect to this, three samples, namely pristine chitosan (>1000 nm), NCS2 (ca. 336 nm, 20 min treatment, 40% amplitude) and NCS7 (ca. 77 nm, 120 min treatment, 70% amplitude), were selected and measured. These three samples were selected because they possessed significantly different sizes under substantial different synthesis conditions. The XRD data (Figure 3) show that the pristine chitosan sample exhibit two broad peaks at $2\theta = 9.86^\circ$ (due to amine I “–N–CO–CH₃” of

chitosan) and 19.84° (due to amine II “-NH₂” of chitosan), indicating its β -semicrystalline structure [38,39]. When the NCS2 solid was irradiated with 40% amplitude of ultrasonic wave for 20 min, two new XRD peaks started to appear at $2\theta = 21.93^\circ$ and 26.68° , revealing the alteration of molecular arrangement in the chitosan solid. In addition, the broadened XRD peaks indicate small crystallites [40]. Further increasing the ultrasonic radiation led to the emerging of new XRD signals at $2\theta = 11.68^\circ$, 12.76° , 16.88° , 19.18° , 22.86° , 30.04° , etc., showing the change of crystalline structure in NCS7 sample. It is suggested that a long ultrasonication treatment with intense radiation (high amplitude and energy) can easily break down the polymeric chain of chitosan, forming a smaller unit of chitosan. According to Vivekanandan et al. [41], there are two main factors that govern the crystallinity of chitosan, viz. the nature of structure and orientation of chitosan. When the chitosan particle size is reduced to nanometer size, the crystallinity tends to be improved due to the fact that the uniform molecular structure has been formed. In addition, these crystalline chitosan nanoparticles also tend to arrange themselves in preferential orientation (side-to-side or head-to-head) via positive-negative partial charges interaction. As a result, the combination of the crystalline nature of chitosan nanoparticles with preferential orientation contributes to the high crystallinity in the XRD pattern. This phenomenon is also observed and is in good agreement with the previous reports [42,43].

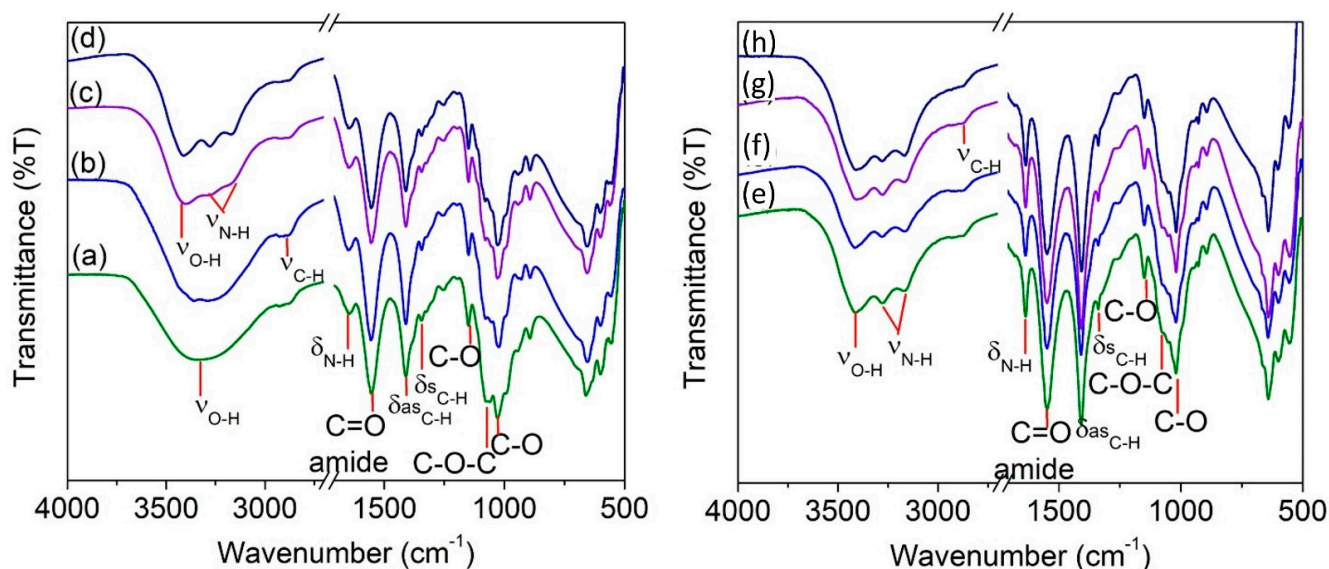


Figure 2. FTIR spectra of (a) pristine chitosan, (b) NCS1, (c) NCS2, (d) NCS3, (e) NCS4, (f) NCS5, (g) NCS6 and (h) NCS7 samples where ν = stretching, δ = bending, δ_s = symmetrical bending and δ_{as} = asymmetrical bending modes.

The XRD observation is further supported by the SEM and TEM data. It can be seen that the pristine chitosan is composed of agglomerated bulk particles above $1\ \mu\text{m}$ (Figure 4a). The agglomerates started to breakdown into smaller NCS2 particles after 20 min of ultrasonication (40% amplitude) (Figure 4b). Further extending the treatment time to 120 min using 40% ultrasonic amplitude successfully produced chitosan nanoparticles with an average size of 110 nm (Figure 4c). Meanwhile, increasing the amplitude of ultrasonic wave also showed a reduction in the particle size. For instance, NCS7 (70% amplitude, 120 min) exhibits nanoparticles of spherical morphology with a smaller size of ca. 78 nm (Figure 4d–f). Hence, both the SEM and XRD data indicate that the ultrasonic synthesis is a promising approach for the preparation of chitosan nanoparticles.

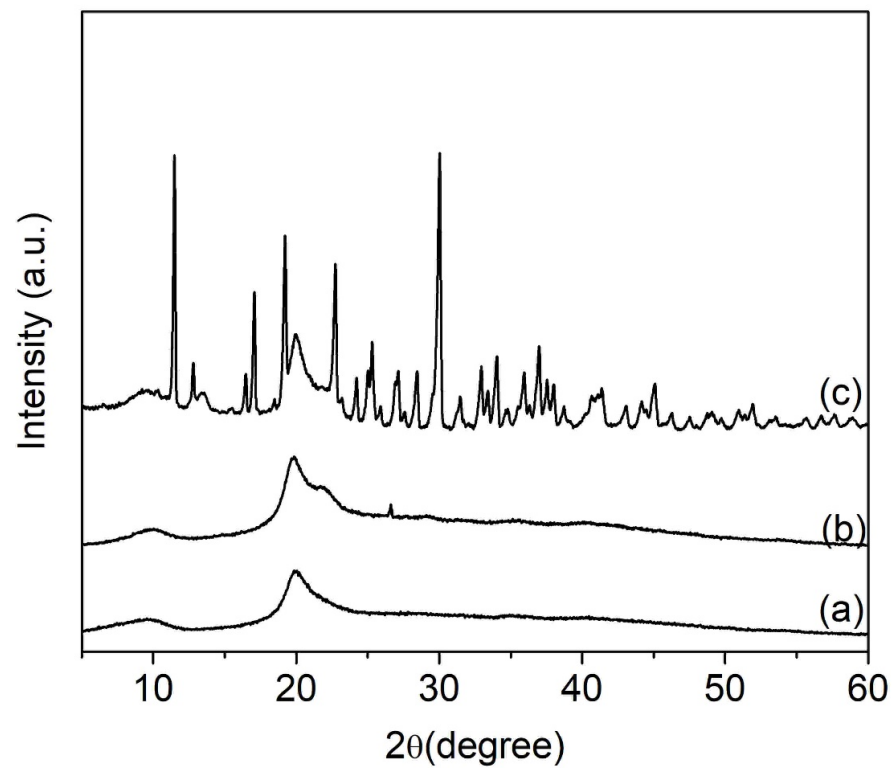


Figure 3. XRD patterns of (a) pristine, (b) NCS2 and (c) NCS7 chitosan samples.

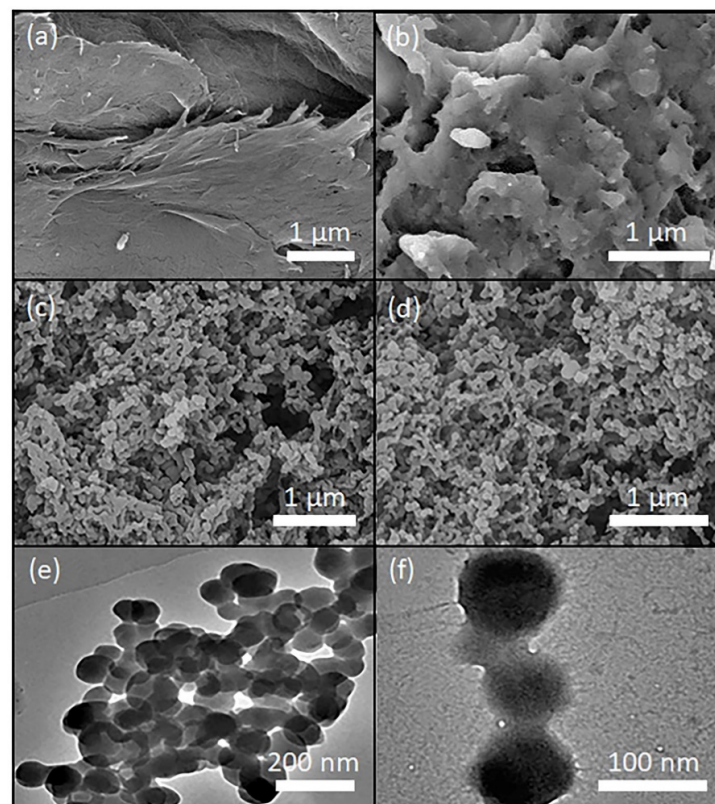


Figure 4. SEM images of (a) pristine, (b) NCS2, (c) NCS4 and (d) NCS7 chitosan samples. The TEM images of NCS7 are shown in (e,f).

3.4. Coagulation Performance in Wastewater Treatment

3.4.1. Turbidity Removal Efficiency

Chitosan particles (pristine, NCS1–NCS7) were tested as bio-coagulants/flocculants in wastewater treatment, where the water from Citarum river—one of the most polluted river in Java Island due to forestry industry—was investigated [44]. The initial wastewater was a cloudy sample due to the presence of many colloidal dispersed clay particles (Figure 5a). The sample also shows a weak acidic pH (6.52), high alkalization (423.1 mg/mL as CaCO₃) and high turbidity (148.2 NTU) values. However, when the water samples were treated with pristine chitosan (as control) and nanosized chitosan solids, the water became less cloudy, showing the good potential of chitosan as an eco-friendly bio-coagulant/flocculant. It is noteworthy that the water samples treated with NCS4, NCS5, NCS6 and NCS7 showed the highest degree of clarity (Figure 5b–i). The turbidity removal performance was also quantitatively measured using the jar test. In general, the data are fully in line with the visual observation (Figure 6). As shown, the residual turbidity value of wastewater dropped drastically from 148.2 NTU to 95.7 NTU, with a recorded turbidity removal efficiency of 35.4% when pristine chitosan was used in the coagulation/flocculation process. The turbidity removal efficiency was enhanced substantially when the water was treated with chitosan nanoparticles where the particle size showed a positive effect on the coagulation/flocculation performance. Among the chitosan nanoparticles samples tested, NCS7, with the particle sizes of ca. 77 nm, had the best turbidity removal performance (ca. 75%). In the absence of any coagulant/flocculant, the clay particles tend to be colloiddally suspended in water due to interaction forces (e.g., interfacial free energy) between the particles and water. As a result, a stable cloudy water suspension is formed. The stability of colloidal system, however, is interrupted when chitosan nanoparticles with positive charge are introduced, where the negatively charged colloidal clay particles tend to interact with the counter charged chitosan nanoparticles. As a result, the colloids in water are destabilized, which facilitates clay particles' coagulation and sedimentation that further leads to a reduction in turbidity (Figure 5) [45,46]. Moreover, the discrete and small particle size of chitosan also provides greater surface contact area for allowing colloidal clay particles to interact with the bio-matrix, leading to fast coagulation/flocculation and high turbidity removal [47].

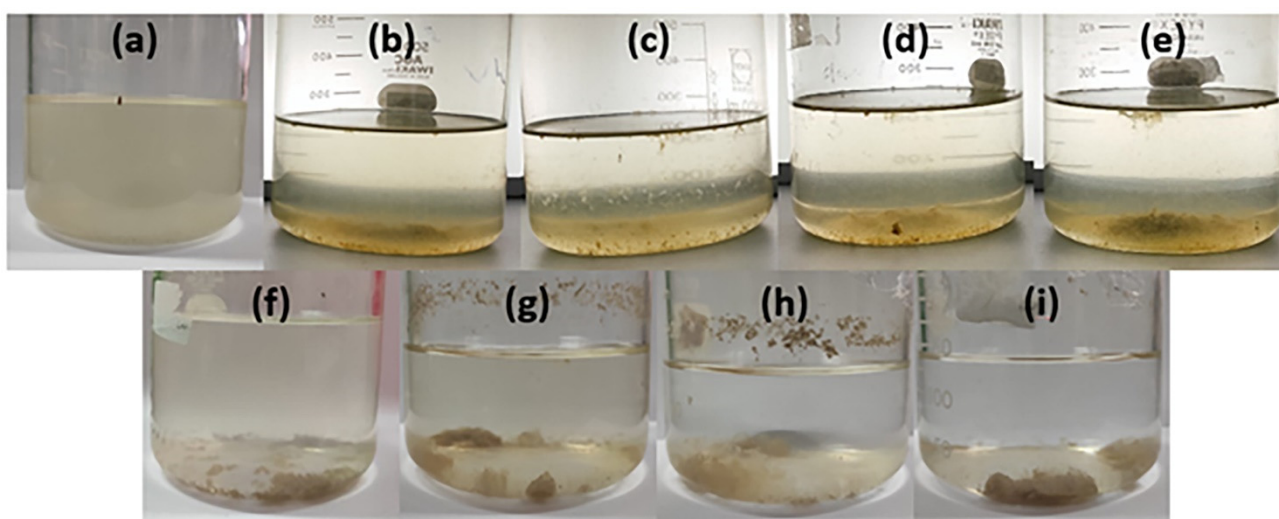


Figure 5. Physical appearance of water samples (a) before and after treatment with (b) pristine chitosan, (c) NCS1, (d) NCS2, (e) NCS3, (f) NCS4, (g) NCS5, (h) NCS6 and (i) NCS7 chitosan nanoparticles.

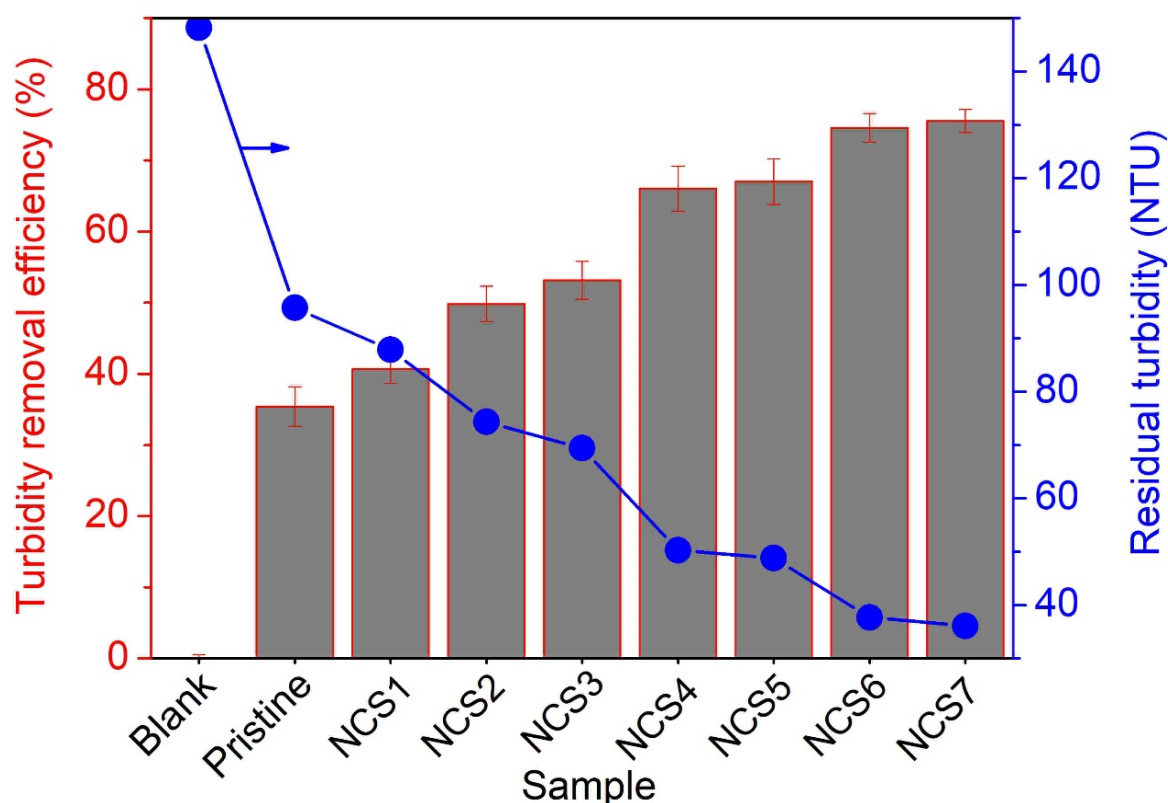


Figure 6. Turbidity removal performance of pristine and nanosized chitosan solids where the turbidity removal efficiency (left) and residual turbidity values (right) are presented.

3.4.2. Dealkalization

Carbonate, bicarbonate and hydroxide of alkaline earth metals, which exist in soluble or sparingly soluble forms, are the key factors controlling the hardness of water. Hence, dealkalization (or demineralization) of alkaline earth metal residues in wastewater treatment is another important process of interest. In respect to this, seven samples of chitosan were investigated in this process. Figure 7 illustrates the dealkalization results of wastewater samples where the alkalinity value of raw wastewater was 423.5 mg/mL as CaCO_3 . With using pristine chitosan as a control and a coagulant/flocculant, the value only dropped to 376.1 mg/mL as CaCO_3 (% dealkalization = 8.8%). A remarkable decrease, however, was seen after the water was treated with a series of chitosan nanoparticles, especially using the NCS7 sample, which had the highest dealkalization (176.3 mg/mL as CaCO_3 , 58.3%) recorded. It is known that the removal of hardness of water (or dealkalization) is associated with the removal of carbonate, bicarbonate and hydroxide of alkaline earth metals, whereby the removal performance is governed by the ionic interactions between the ions and the adsorption sites (protonated surface) of chitosan. When the chitosan particles exist in nanometer scale (especially NCS7), the adsorption efficiency of carbonate, bicarbonate and hydroxide anions is further enhanced as small particle size provides large surface contact area (or high surface charge density) for the removal of hydroxides, bicarbonates and carbonates. As a result, the water is demineralized, creating a softened water stream with low turbidity [10,48]. Thus, the ultrasonication synthesis approach offers an alternative strategy to prepare chitosan nanoparticles without using any harmful and expensive chemicals, where the synthesized chitosan nanoparticles also have great potential in wastewater treatment, particularly in residual turbidity removal and dealkalization technologies.

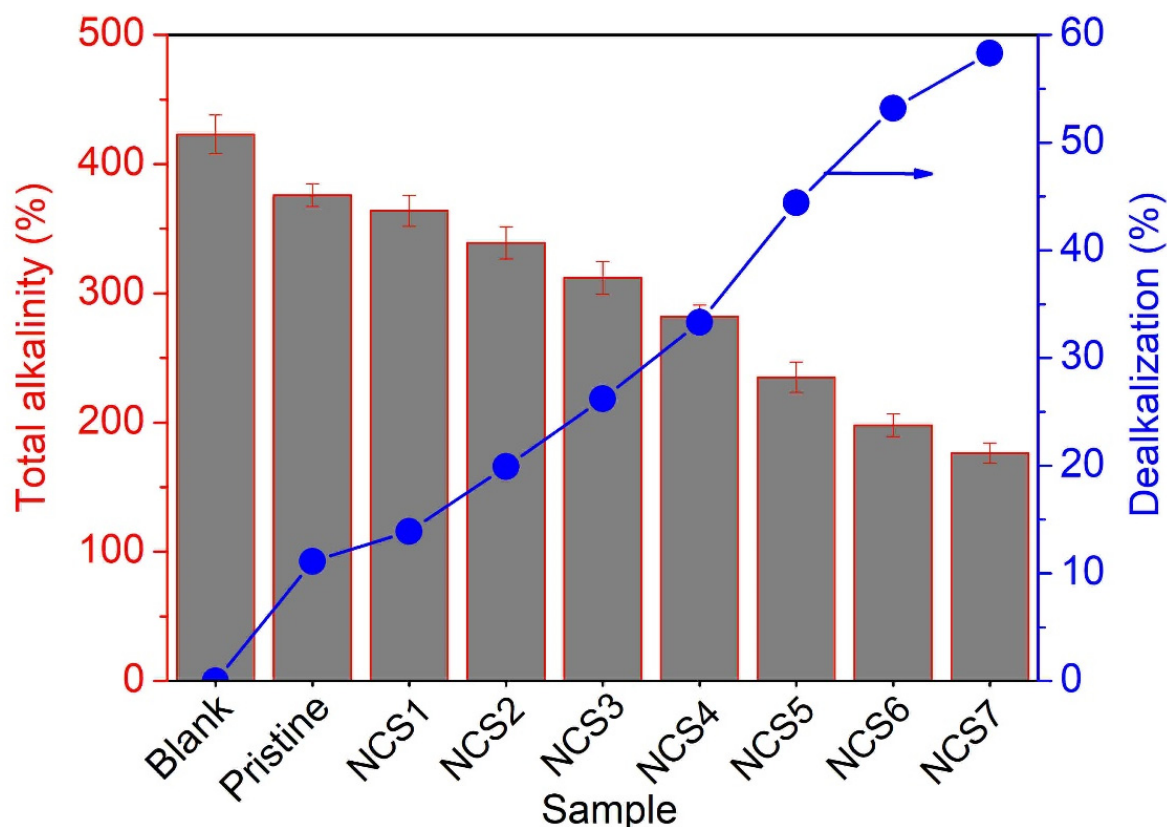


Figure 7. Total alkalinity and dealkalization of wastewater before and after coagulation/flocculation treatment by chitosan bulk and nanoparticles.

4. Conclusions

In conclusion, chitosan nanoparticles have successfully been synthesized under ultrasonication conditions. The results show that increasing ultrasonic amplitude and exposure time, where both parameters are important in the breakdown of chemical bonds and microaggregates, gives rise to the formation of discrete and small crystallites. Among the seven samples prepared, the NCS7 (120 min ultrasonic treatment, 70% amplitude) exhibits the smallest crystallite size with narrow particle size distribution (77.47 ± 28.81). In addition, the chitosan nanoparticles have been shown to be excellent biocoagulant/bioflocculant and dealkalization agents, as very high turbidity removal efficiency (75.5%) and demineralization (58.3%) were achieved by the NCS-7 sample, thus offering a green alternative to the existing water treatment system.

Author Contributions: F.K.: Conceptualization, Methodology, Writing—Original Draft, Funding Acquisition. Y.D.Y.: Investigation, Formal Analysis, Writing—Original Draft. M.N. (Mita Nurhayati): Visualization. F.Z. and M.-Y.C.: Investigation, Formal Analysis. M.N. (Muhamad Nasir): Resources. P.O.: Resources E.-P.N.: Conceptualization, Methodology, Writing—Review and Editing, Supervision. All authors have read and agreed to the published version of the manuscript.

Funding: This research was funded by World Class University (WCU) Program by Ministry of Education and Culture of Republic Indonesia (2021), Fundamental Research Grants (273/UN40.LP/PT.01.03/2021), Intellectual property rights-oriented research (674/UN40.LP/PT.01.03/2021), and UPI research grant (1060/UN40/PT.01.02/2021).

Institutional Review Board Statement: Not applicable.

Informed Consent Statement: Not applicable.

Data Availability Statement: Not applicable.

Acknowledgments: This study was supported by the World Class University (WCU) Program by Ministry of Education and Culture of Republic Indonesia (2021), Fundamental Research Grants (273/UN40.LP/PT.01.03/2021), Intellectual property rights-oriented research (674/UN40.LP/PT.01.03/2021), and UPI research grant (1060/UN40/PT.01.02/2021).

Conflicts of Interest: The authors declare no conflict of interest.

References

1. Agbovi, H.K.; Wilson, L.D. Design of amphoteric chitosan flocculants for phosphate and turbidity removal in wastewater. *Carbohydr. Polym.* **2018**, *189*, 360–370. [[CrossRef](#)] [[PubMed](#)]
2. Saleh, I.A.; Zouari, N.; Al-Ghouti, M.A. Removal of pesticides from water and wastewater: Chemical, physical and biological treatment approaches. *Environ. Technol. Innov.* **2020**, *19*, 101026. [[CrossRef](#)]
3. Vijayalakshmi, K.; Devi, B.M.; Latha, S.; Gomathi, T.; Sudha, P.N.; Venkatesan, J.; Anil, S. Batch adsorption and desorption studies on the removal of lead (II) from aqueous solution using nanochitosan/sodium alginate/microcrystalline cellulose beads. *Int. J. Biol. Macromol.* **2017**, *104*, 1483–1494. [[CrossRef](#)]
4. Chen, Y.; Nakazawa, Y.; Matsui, Y.; Shirasaki, N.; Matsushita, T. Sulfate ion in raw water affects performance of high-basicity PACI coagulants produced by Al(OH)₃ dissolution and base-titration: Removal of SPAC particles by coagulation-flocculation, sedimentation, and sand filtration. *Water Res.* **2020**, *183*, 116093. [[CrossRef](#)]
5. Quinlan, P.J.; Tanvir, A.; Tam, K.C. Application of the central composite design to study the flocculation of an anionic azo dye using quaternized cellulose nanofibrils. *Carbohydr. Polym.* **2015**, *133*, 80–89. [[CrossRef](#)] [[PubMed](#)]
6. Wang, S.-Y.; Fang, L.-F.; Cheng, L.; Jeon, S.; Kato, N.; Matsuyama, H. Novel ultrafiltration membranes with excellent antifouling properties and chlorine resistance using a poly(vinyl chloride)-based copolymer. *J. Membr. Sci.* **2018**, *549*, 101–110. [[CrossRef](#)]
7. Ayoub, M.; Afify, H.; Abdelfattah, A. Chemically enhanced primary treatment of sewage using the recovered alum from water treatment sludge in a model of hydraulic clari-flocculator. *J. Water Process Eng.* **2017**, *19*, 133–138. [[CrossRef](#)]
8. Ucevlı, O.; Kaya, Y. A comparative study of membrane filtration, electrocoagulation, chemical coagulation and their hybrid processes for greywater treatment. *J. Environ. Chem. Eng.* **2021**, *9*, 104946. [[CrossRef](#)]
9. Owodunni, A.A.; Ismail, S. Revolutionary technique for sustainable plant-based green coagulants in industrial wastewater treatment—A review. *J. Water Process Eng.* **2021**, *42*, 102096. [[CrossRef](#)]
10. W. Pontius, F. Chitosan as a Drinking Water Treatment Coagulant. *Am. J. Civ. Eng.* **2016**, *4*, 205. [[CrossRef](#)]
11. Khoerunnisa, F.; Rahmah, W.; Seng Ooi, B.; Dwihermiati, E.; Nashrah, N.; Fatimah, S.; Ko, Y.G.; Ng, E.P.; Khoerunnisa, F. Chitosan/PEG/MWCNT/Iodine composite membrane with enhanced antibacterial properties for dye wastewater treatment. *J. Environ. Chem. Eng.* **2020**, *8*, 103686. [[CrossRef](#)]
12. Khoerunnisa, F.; Nurhayati, M.; Dara, F.; Rizki, R.; Nasir, M.; Aziz, H.A.; Hendrawan, H.; Ng, E.P.; Kaewsaneha, C.; Opaprakasit, P. Physicochemical Properties of TPP-Crosslinked Chitosan Nanoparticles as Potential Antibacterial Agents. *J. Colloid Interface Sci.* **2021**, *22*, 225–235. [[CrossRef](#)]
13. Islam, S.; Bhuiyan, M.A.R.; Islam, M.N. Chitin and Chitosan: Structure, Properties and Applications in Biomedical Engineering. *J. Polym. Environ.* **2017**, *25*, 854–866. [[CrossRef](#)]
14. Mohammed, I.A.; Jawad, A.H.; Abdulhameed, A.S.; Mastuli, M.S. Physicochemical modification of chitosan with fly ash and tripolyphosphate for removal of reactive red 120 dye: Statistical optimization and mechanism study. *Int. J. Biol. Macromol.* **2020**, *161*, 503–513. [[CrossRef](#)] [[PubMed](#)]
15. Saheed, I.O.; Oh, W.D.; Suah, F.B.M. Chitosan modifications for adsorption of pollutants—A review. *J. Hazard. Mater.* **2021**, *408*, 124889. [[CrossRef](#)]
16. Iber, B.T.; Okomoda, V.T.; Rozaimah, S.A.; Kasan, N.A. Eco-friendly approaches to aquaculture wastewater treatment: Assessment of natural coagulants vis-a-vis chitosan. *Bioresour. Technol. Rep.* **2021**, *15*, 100702. [[CrossRef](#)]
17. Li, Y.; Yang, Y.; Huang, Z.; Luo, Z.; Qian, C.; Li, Y.; Duan, Y. Preparation of low molecular chitosan by microwave-induced plasma desorption/ionization technology. *Int. J. Biol. Macromol.* **2021**, *187*, 441–450. [[CrossRef](#)]
18. Chavan, P.; Sinhmar, A.; Nehra, M.; Thory, R.; Pathera, A.K.; Sundarraj, A.A.; Nain, V. Impact on various properties of native starch after synthesis of starch nanoparticles: A review. *Food Chem.* **2021**, *364*, 130416. [[CrossRef](#)]
19. Wani, T.U.; Pandith, A.H.; Sheikh, F.A. Polyelectrolytic nature of chitosan: Influence on physicochemical properties and synthesis of nanoparticles. *J. Drug Deliv. Sci. Technol.* **2021**, *65*, 102730. [[CrossRef](#)]
20. Sivakami, M.S.; Gomathi, T.; Venkatesan, J.; Jeong, H.; Kim, S.; Sudha, P.N. International Journal of Biological Macromolecules Preparation and characterization of nano chitosan for treatment wastewaters. *Int. J. Biol. Macromol.* **2013**, *57*, 204–212. [[CrossRef](#)]
21. Wonnıe Ma, I.A.; Ammar, S.; Bashir, S.; Selvaraj, M.; Assiri, M.A.; Ramesh, K.; Ramesh, S. Preparation of Hybrid Chitosan/Silica Composites Via Ionotropic Gelation and Its Electrochemical Impedance Studies. *Prog. Org. Coat.* **2020**, *145*, 105679. [[CrossRef](#)]
22. Oliveira, D.A.J.; Amaral, J.G.; Garcia, L.B.; dos Santos, M.S.; Silva, L.A.O.; Almeida, M.P.; Gomes, A.F.; Barros, D.R.P.; Lopes, N.P.; Pereira, G.R.; et al. Associating chitosan and microemulsion as a topical vehicle for the administration of herbal medicines. *Carbohydr. Polym.* **2021**, *255*, 117482. [[CrossRef](#)] [[PubMed](#)]
23. Qin, C.; Zhou, J.; Zhang, Z.; Chen, W.; Hu, Q.; Wang, Y. Convenient one-step approach based on stimuli-responsive sol-gel transition properties to directly build chitosan-alginate core-shell beads. *Food Hydrocoll.* **2019**, *87*, 253–259. [[CrossRef](#)]

24. Soares, P.I.P.; Machado, D.; Laia, C.; Pereira, L.C.J.; Coutinho, J.T.; Ferreira, I.M.M.; Novo, C.M.M.; Borges, J.P. Thermal and magnetic properties of chitosan-iron oxide nanoparticles. *Carbohydr. Polym.* **2016**, *149*, 382–390. [[CrossRef](#)] [[PubMed](#)]
25. Gokce, Y.; Cengiz, B.; Yildiz, N.; Calimli, A.; Aktas, Z. Ultrasonication of chitosan nanoparticle suspension: Influence on particle size. *Colloids Surf. A Physicochem. Eng. Asp.* **2014**, *462*, 75–81. [[CrossRef](#)]
26. Ng, E.P.; Awala, H.; Ghoy, J.P.; Vicente, A.; Ling, T.C.; Ng, Y.H.; Mintova, S.; Adam, F. Effects of ultrasonic irradiation on crystallization and structural properties of EMT-type zeolite nanocrystals. *Mater. Chem. Phys.* **2015**, *159*, 38–45. [[CrossRef](#)]
27. Boufi, S.; Bel Haaj, S.; Magnin, A.; Pignon, F.; Impéror-Clerc, M.; Mortha, G. Ultrasonic assisted production of starch nanoparticles: Structural characterization and mechanism of disintegration. *Ultrason. Sonochem.* **2018**, *41*, 327–336. [[CrossRef](#)]
28. Lobo, C.; Castellari, J.; Colman Lerner, J.; Bertola, N.; Zaritzky, N. Functional iron chitosan microspheres synthesized by ionotropic gelation for the removal of arsenic (V) from water. *Int. J. Biol. Macromol.* **2020**, *164*, 1575–1583. [[CrossRef](#)]
29. Xu, D.; Li, L.; Wu, Y.; Zhang, X.; Wu, M.; Li, Y.; Gai, Z.; Li, B.; Zhao, D.; Li, C. Influence of ultrasound pretreatment on the subsequent glycation of dietary proteins. *Ultrason. Sonochem.* **2020**, *63*, 104910. [[CrossRef](#)]
30. Dai, C.; Yin, Z.; Wang, P.; Miao, Q.; Chen, J. Analysis on ground surface in ultrasonic face grinding of silicon carbide (SiC) ceramic with minor vibration amplitude. *Ceram. Int.* **2021**, *47*, 21959–21968. [[CrossRef](#)]
31. Roohi, R.; Abedi, E.; Hashemi, S.M.B.; Marszałek, K.; Lorenzo, J.M.; Barba, F.J. Ultrasound-assisted bleaching: Mathematical and 3D computational fluid dynamics simulation of ultrasound parameters on microbubble formation and cavitation structures. *Innov. Food Sci. Emerg. Technol.* **2019**, *55*, 66–79. [[CrossRef](#)]
32. Wong, S.F.; Deekomwong, K.; Wittayakun, J.; Ling, T.C.; Muraza, O.; Adam, F.; Ng, E.P. Crystal growth study of K-F nanozeolite and its catalytic behavior in Aldol condensation of benzaldehyde and heptanal enhanced by microwave heating. *Mater. Chem. Phys.* **2017**, *196*, 295–301. [[CrossRef](#)]
33. Sangeetha, V.; Sudha, P.N. Synthesis and characterisation of nano chitosan/PVP/SF for environmental engineering applications. *Int. J. Ambient Energy* **2021**, *42*, 150–155. [[CrossRef](#)]
34. Baklagina, Y.G.; Klechkovskaya, V.V.; Kononova, S.V.; Petrova, V.A.; Poshina, D.N.; Orekhov, A.S.; Skorik, Y.A. Polymorphic Modifications of Chitosan. *Crystallogr. Rep.* **2018**, *63*, 303–313. [[CrossRef](#)]
35. Wu, T.; Wu, C.; Xiang, Y.; Huang, J.; Luan, L.; Chen, S.; Hu, Y. Kinetics and mechanism of degradation of chitosan by combining sonolysis with H₂O₂/ascorbic acid. *RSC Adv.* **2016**, *6*, 76280–76287. [[CrossRef](#)]
36. Brugnerotto, J.; Lizardi, J.; Goycoolea, F.M.; Argüelles-Monal, W.; Desbrières, J.; Rinaudo, M. An infrared investigation in relation with chitin and chitosan characterization. *Polymer* **2001**, *42*, 3569–3580. [[CrossRef](#)]
37. Joseph, D.; Cruz-romero, M.; Collins, T.; Cummins, E.; Kerry, J.P.; Morris, M.A. Food Hydrocolloids Synthesis of monodisperse chitosan nanoparticles. *Food Hydrocoll.* **2018**, *83*, 355–364.
38. Jampafuang, Y.; Tongta, A.; Waiprib, Y. Impact of crystalline structural differences between α - and β -chitosan on their nanoparticle formation via ionic gelation and superoxide radical scavenging activities. *Polymers* **2019**, *11*, 2010. [[CrossRef](#)]
39. Muley, A.B.; Chaudhari, S.A.; Mulchandani, K.H.; Singhal, R.S. Extraction and characterization of chitosan from prawn shell waste and its conjugation with cutinase for enhanced thermo-stability. *Int. J. Biol. Macromol.* **2018**, *111*, 1047–1058. [[CrossRef](#)]
40. Maniammal, K.; Madhu, G.; Biju, V. X-ray diffraction line profile analysis of nanostructured nickel oxide: Shape factor and convolution of crystallite size and microstrain contributions. *Phys. E Low-Dimens. Syst. Nanostruct.* **2017**, *85*, 214–222. [[CrossRef](#)]
41. Vivekanandan, K.E.; Swethavinayagam, S.; Venkatesan, D.; Rebecca, L.J. Preparation of Chitosan Nanoparticles and its Synergistic Effects against Gram Positive and Gram Negative Microorganisms. *J. Pure Appl. Microbiol.* **2019**, *13*, 2317–2324. [[CrossRef](#)]
42. Morsy, M.; Mostafa, K.M.; Amyn, H.A.M.; El-Ebissy, A.A.-H.; Salah, A.M.; Youssef, M.A. Synthesis and characterization of freeze dryer chitosan nanoparticles as multifunctional eco-friendly finish for fabricating easy care and antibacterial cotton textiles. *Egypt. J. Chem.* **2019**, *62*, 1277–1293.
43. Kaur, P.; Choudhary, A.; Thakur, R. Synthesis of chitosan-silver nanocomposites and their antibacterial activity. *Int. J. Sci. Eng. Res.* **2013**, *4*, 869.
44. Bainus, A.; Darmawan, W.B.; Yulianti, D.; Husin, L.H. Between fear and survival: Human security issues in Citarum River Basin, Indonesia. *J. Hum. Secur.* **2021**, *17*, 4–14. [[CrossRef](#)]
45. Kumar, S.; Ye, F.; Dobretsov, S.; Dutta, J. Chitosan nanocomposite coatings for food, paints, and water treatment applications. *Appl. Sci.* **2019**, *9*, 2409. [[CrossRef](#)]
46. Meraz, K.A.S.; Vargas, S.M.P.; Maldonado, J.T.L.; Bravo, J.M.C.; Guzman, M.T.O.; Maldonado, E.A.L. Eco-friendly innovation for nejayote coagulation–flocculation process using chitosan: Evaluation through zeta potential measurements. *Chem. Eng. J.* **2016**, *284*, 536–542. [[CrossRef](#)]
47. Xu, Y.; Dang, Q.; Liu, C.; Yan, J.; Fan, B.; Cai, J.; Li, J. Preparation and characterization of carboxyl-functionalized chitosan magnetic microspheres and submicrospheres for Pb²⁺ removal. *Colloids Surf. A Physicochem. Eng. Asp.* **2015**, *482*, 353–364. [[CrossRef](#)]
48. Mukhopadhyay, R.; Adhikari, T.; Sarkar, B.; Barman, A.; Paul, R.; Patra, A.K.; Sharma, P.C.; Kumar, P. Fe-exchanged nanobentonite outperforms Fe₃O₄ nanoparticles in removing nitrate and bicarbonate from wastewater. *J. Hazard. Mater.* **2019**, *376*, 141–152. [[CrossRef](#)]